

iMHS: An Incremental Multi-Hypothesis Smoother

Fan Jiang, Varun Agrawal, Russell Buchanan, Maurice Fallon, and Frank Dellaert

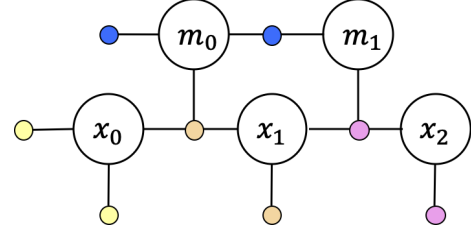
Abstract—State estimation of multi-modal hybrid systems is an important problem with many applications in the field robotics. However, incorporating discrete modes in the estimation process is hampered by a potentially combinatorial growth in computation. In this paper we present a novel *incremental* multi-hypothesis smoother based on eliminating a hybrid factor graph into a multi-hypothesis Bayes tree, which represents possible discrete state sequence hypotheses. Following iSAM, we enable incremental inference by conditioning the past on the future but we add to that the capability of maintaining multiple discrete mode histories, exploiting the temporal structure of the problem to obtain a simplified representation that unifies the multiple hypothesis tree with the Bayes tree. In the results section we demonstrate the generality of the algorithm with examples in three problem domains: lane change detection (1D), aircraft maneuver detection (2D), and contact detection in legged robots (3D).

I. INTRODUCTION

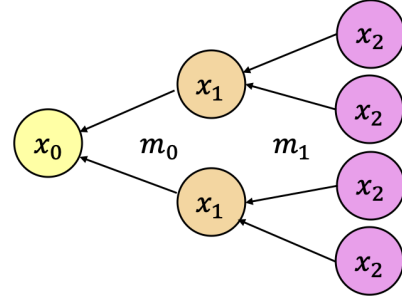
State estimation of multi-modal hybrid systems is an important problem with many compelling applications. A sample of these applications include fault detection [7], [9]), air traffic control (ATC) [11], [29], decoding cortical motor activity [28], and contact dynamics in legged robots [8]. In the last example, accurate determination of contact state in manipulation and/or walking is challenging yet vital when executing accurate manipulation or locomotion plans.

However, incorporating discrete modes in the estimation process suffers from combinatorial growth in computation. Hence, there is a long history of work on filtering-based approaches, the most well-known of which are model adaptive estimation (MMAE) [18] and the interacting multiple model (IMM) [1]. This line of work has been further expanded to switching dynamics Bayes nets by Murphy [19], [20]. Optimizing over the entire time history or *smoothing* is much more challenging, although it has been approximated using Markov Chain Monte Carlo (MCMC) sampling [23], [22] and variational inference [6]. Various methods which keep track of sets of hypotheses has been proposed in the multi-target tracking literature, including the now classical multiple hypothesis tracking (MHT) filter [24], [4], the probabilistic MHT [25], JPDAF [1]. Both particle-filtering [26] and MCMC smoothing [16], [17], [21] have been applied.

In this paper we present a novel *incremental* multi-hypothesis smoother based on eliminating a hybrid factor



(a) Factor graph for hybrid switching system, with continuous states x_k evolving according to discrete modes m_k .



(b) The proposed multi-hypothesis smoother conditions the past on the future in parallel branches of a tree.

Fig. 1: The iMHS concept illustrated for a toy example.

graph into a multi-hypothesis Bayes tree, which represents possible discrete state sequence hypotheses. We base our work on iSAM [15], [13], which enables incremental inference by conditioning the past on the future, but we add to that the capability of maintaining multiple discrete mode histories. In contrast to sampling-based and variational approaches, the computational cost is bounded by meaningful thresholds on the probability of state histories, and incremental inference is constant-time. While our approach is similar in spirit to MH-iSAM2 by Hsiao and Kaess [10], we exploit the temporal structure of the problem to obtain a simplified representation that unifies the multiple hypothesis tree with the Bayes tree. In addition, we support stochastic transitions over the mode sequence, and can properly handle model selection when modes are not all equally informative about the dynamics or measurement models.

A small example in Figure 1 demonstrates the basic idea. The batch problem is represented as a factor graph with the state at three time instants, and a Markov chain of discrete modes that select a different process model at each time step. The unary factors are measurements and will help determine which process model is most likely. In the case of a binary mode variable, the mode selects between

Institute for Robotics and Intelligent Machines, College of Computing, Georgia Institute of Technology, Atlanta, GA, {fan.jiang,varunagrawal,frank.dellaert}@gatech.edu
Oxford Robotics Institute, Department of Engineering Science, University of Oxford, Oxford, UK, {mfallon,russell}@robots.ox.ac.uk

The NASA University Leadership Initiative (grant #80NSSC20M0163) provided funds to assist the authors with their research, but this article solely reflects the opinions and conclusions of its authors and not any NASA entity.

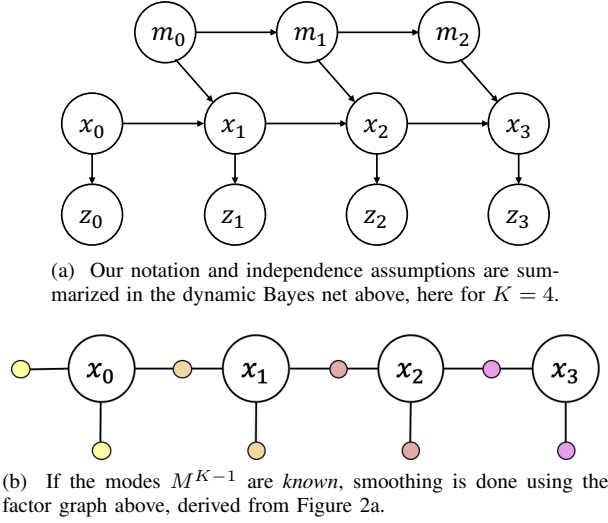


Fig. 2: Notation and independence assumptions.

two process models. For this example with $K = 3$ states there are eight possible discrete mode sequences. A naive algorithm would eliminate the factor graph separately for each sequence. However, Figure 1b shows that the eliminated factor graphs can be combined into a multiple-hypothesis tree of conditionals, conditioned on the future states.

In the results section we show examples from vehicle lane-change detection, aircraft tracking, and contact estimation of legged robots, all of which can be modeled in the above framework. In general, any system described by a dynamic Bayes net with a combination of discrete and continuous variables can be accommodated.

In summary, the contributions of this work are:

- A novel, incremental smoother algorithm for hybrid/multi-modal systems.
- A novel data structure that unifies multiple hypothesis trees and Bayes trees.
- A demonstration of the generality of the algorithm with examples in three problem domains: lane change detection (1D), aircraft maneuver detection (2D), and contact detection in legged robots (3D).

II. BACKGROUND

In this paper we rely heavily on the use of graphical models, including dynamic Bayes nets, factor graphs, and incremental inference, which we will review in this section.

A. Problem statement and notation

Continuous smoothing is the problem of recovering the posterior density

$$p(X^K | M^{K-1}, Z^K), \quad (1)$$

where $X^K \doteq \{x_k\}_{k=0}^{K-1}$ is a sequence of K states from time t_0 up to and including time t_{K-1} , with $x_k \in \mathcal{X}$ representing the state at time t_k . Given a similarly defined sequence of discrete modes M^{K-1} and measurements Z^K , with $m_k \in$

\mathcal{M} and $z_k \in \mathcal{Z}$, we model the joint density over all variables using the following dynamic Bayes net [20] (Figure 2a):

$$p(X^K, M^{K-1}, Z^K) = P(x_0)p(z_0|x_0)p(m_0) \times \prod_{k=1}^{K-1} p(m_k, x_k, z_k | m_{k-1}, x_{k-1}). \quad (2)$$

We assume the mode sequence M^{K-1} is modeled by a Markov chain $P(m_k | m_{k-1})$. The continuous states evolve via a switching motion model $p(x_k | x_{k-1}, m_{k-1})$, and measurements are modeled on the continuous states as $p(z_k | x_k)$. One time slice in the dynamic Bayes net is given by

$$p(m_k, x_k, z_k | m_{k-1}, x_{k-1}) = P(m_k | m_{k-1})p(x_k | x_{k-1}, m_{k-1})p(z_k | x_k). \quad (3)$$

B. Factor Graphs and Trajectory Optimization

When both discrete modes M^{K-1} and measurements Z^K are known, it is convenient to represent the posterior density (1) using a factor graph [5] as illustrated in Figure 2b,

$$\begin{aligned} \phi(X^K) &\propto p(X^K | M^{K-1}, Z^K) \\ &\doteq \phi(x_0)\phi_0^z(x_0) \prod_{k=1}^{K-1} \phi_k^m(x_{k-1}, x_k)\phi_k^z(x_k) \end{aligned} \quad (4)$$

with the factors defined in correspondence with (2).

The maximum a posteriori (MAP) estimate can be recovered by maximizing $\phi(X^K)$ with respect to the continuous states X^K , also known as trajectory optimization:

$$X^{K*} = \arg \min_{X^K} \phi(X^K). \quad (5)$$

By fitting a quadratic to the log-posterior, e.g., using the estimate $A^T A$ to the Fisher information matrix \mathcal{I} , where

$$A \doteq -\frac{\partial \log \phi(X^K)}{\partial X^K}, \quad (6)$$

we can obtain an approximation to the posterior as

$$p(X^K | M^{K-1}, Z^K) \approx \mathcal{N}(X^K; X^{K*}, \mathcal{I}^{-1}), \quad (7)$$

where $\mathcal{N}(x; \mu, \Sigma) \propto \exp \{-0.5\|x - \mu\|_{\Sigma}^2\}$ is the multivariate normal distribution with mean μ and covariance Σ .

C. The linear case: Kalman smoothing

In the common case when all continuous densities are linear-Gaussian and (w.l.o.g.) time invariant, we have

$$p(x_k | x_{k-1}, m) = \mathcal{N}(x_k; F_m x_{k-1} + B_m u_{k-1}, Q_m) \quad (8)$$

$$p(z_k | x_k, m) = \mathcal{N}(z_k; H_m x_k, R_m) \quad (9)$$

with a vector-valued state $X^K \in R^n$, a control vector $u^k \in R^p$, and a vector-valued measurement $z_k \in R^m$. Matrices F_m , B_m , and H_m , as well as the process and noise covariances Q_m and R_m can depend on the mode m . It is convenient to define factors in negative log-space, and to

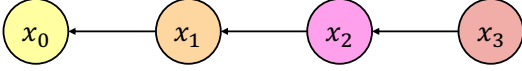


Fig. 3: Bayes net representation of posterior $p^*(X^K)$, conditioning the past on the future to enable incremental inference.

minimize the following least-squares criterion, defined as an additive factor graph:

$$\begin{aligned} f(X^K) &\doteq -\log \phi(X^K) \\ &= f_0^m(x_0) + \sum_{k=1}^{K-1} f_k^m(x_{k-1}, x_k) + \sum_{k=0}^{K-1} f_k^z(x_k) \end{aligned} \quad (10)$$

with quadratic factors $f(\cdot) \doteq -\log \phi(\cdot)$ defined as

$$f_1^m(x_0) = \|x_0 - \mu\|_P^2 \quad (11)$$

$$f_k^m(x_{k-1}, x_k) = \|x_k - (F_m x_{k-1} + B_m u_{k-1})\|_{Q_m}^2 \quad (12)$$

$$f_k^z(x_k) = \|H_m x_k - z_k\|_{R_m}^2. \quad (13)$$

In this case the approximation (7) is exact, with A the sparse Jacobian of $f(X^K)$, and the mean X^{K*} . These can be found in closed form by solving the normal equations

$$(A^T A) X^{K*} = A^T b \quad (14)$$

with the right-hand side (RHS) b suitably defined.

D. Incremental Inference

Recovering the posterior $p^*(X^K)$ -solving the normal equations in the linear case- can be done using sparse elimination [5]. If we eliminate with a natural, time-aligned ordering then under our assumptions the posterior density $p^*(X^K) \doteq p(X^K | M^{K-1}, Z^K)$ will have the form of a chain of conditional densities,

$$p^*(X^K) = \left\{ \prod_{k=1}^{K-1} p^*(x_{k-1} | x_k) \right\} p^*(x_{K-1}), \quad (15)$$

where we use $*$ to indicate that these are conditioned on the measurements and mode sequence. As illustrated in Figure 3, with this factorization the past is conditioned on the future, which enables a simple incremental inference scheme.

The goal of incremental inference is to obtain the posterior density $p^*(X^{K+1})$ at the next time step given the current posterior density $p^*(X^K)$, the new discrete mode m_{K-1} , and a new measurement z_K :

$$p(X^{K+1} | M^K, Z^{K+1}) \leftarrow p(X^K | M^{K-1}, Z^K) \quad (16)$$

Following iSAM2 [13] it suffices to assemble the following factor graph fragment

$$\phi(x_{K-1}) \phi_k^m(x_{K-1}, x_K) \phi_K^z(x_K) \quad (17)$$

where the first factor $\phi(x_{K-1})$ corresponds to the density $p^*(x_{K-1})$ from (15). We then eliminate this into a replacement for $p^*(x_{K-1})$, obtaining two conditionals:

$$p^*(x_{K-1} | x_K) p^*(x_K). \quad (18)$$

In the linear case, the incremental update can be done in square-root information form using QR factorization [2], [14]:

$$U \left[\begin{array}{cc|c} A_{K-1} & -F_m & b_{K-1} \\ I_n & H_m & z_K \end{array} \right] \rightarrow \left[\begin{array}{cc|c} R_m & S_m & u_m \\ & T_m & v_m \\ & & e_m \end{array} \right] \quad (19)$$

where the left matrix, augmented with its RHS, corresponds to the factor graph fragment, and $U \doteq \text{diag}(P, Q_m, R)^{-0.5}$ collects the noise covariances. The upper-triangular matrix on right, also with RHS, corresponds to the resulting Bayes net fragment (18). Extracting the latter yields the two Gaussian conditional densities on X_K and x_K :

$$\begin{aligned} p^*(x_{K-1} | x_K) &= \mathcal{N}(x_{K-1}; R_m^{-1}(u_m - S_m x_K), R_m^{-1} R_m^{-T}) \\ p^*(x_K) &= \mathcal{N}(x_K; T_m^{-1} v_m, T_m^{-1} T_m^{-T}). \end{aligned} \quad (20)$$

When the factor graph fragment matrix has rank exactly $2n$, the error at the minimum of the associated quadratic is zero; otherwise, it is $0.5 e_m^T e_m$. We will use this result below.

In the nonlinear case, iSAM [15] and iSAM2 [13] provide incremental management of linearization points, and also handle more general factor graph topologies.

III. APPROACH

All of the above assumed known hybrid modes, in which case incremental smoothing is both well known and efficient. In this section we present the main contribution of the paper, which uses a multiple hypothesis framework to effectively run many smoothers in parallel, but arranged in a tree to accommodate shared history. The probability of a particular mode sequence depends both on a Markov chain prior *and* on how compatible the estimated continuous state trajectory is with a particular mode sequence. For example, in a lane change scenario, the changing lateral position of the car provides evidence that a lane change maneuver is in progress.

A. Hybrid State Estimation

When the hybrid modes M^{K-1} are unknown, we have a hybrid state estimation problem. In this section, we add the mode sequence M^{K-1} as unknowns to the factor graph:

$$\begin{aligned} \phi(X^K, M^{K-1}) &\doteq \phi(m_0) \phi(x_0) \phi_0^z(x_0) \\ &\times \prod_{k=1}^{K-1} \phi(m_{k-1}, m_k) \phi(x_{k-1}, x_k, m_k) \phi_k^z(x_k) \end{aligned} \quad (21)$$

Above we added a prior on m_0 , a mode transition model $\phi(m_{k-1}, m_k)$, and the motion model factors $\phi_k^m(x_{k-1}, x_k, m_k)$ are now also a function of the mode m_k .

Within a batch smoother, when we eliminate the states X^K with the oldest time-aligned ordering, and *then* eliminate the entire mode sequence, we can obtain a chain of state densities $p(x_{k-1} | x_k, M^k)$ conditioned on the future, and on the mode

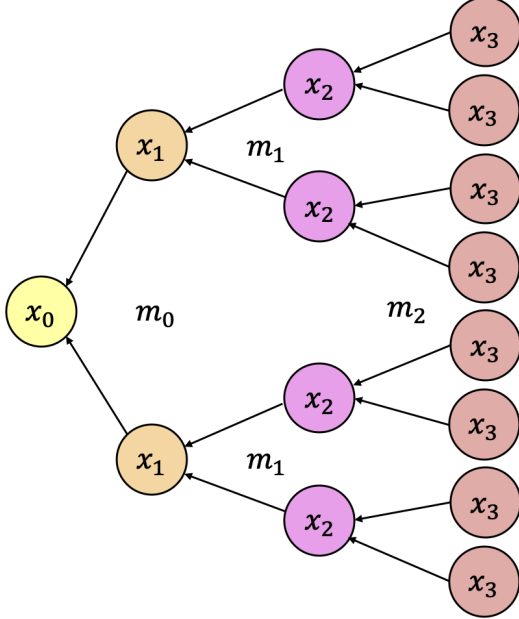
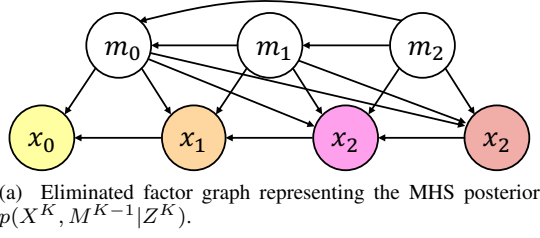


Fig. 4: Classic Bayes net vs. tree-structured smoother.

variables M^k up to that time:

$$p(X^K, M^{K-1} | Z^K) = \left\{ \prod_{k=1}^{K-1} p^*(x_{k-1} | x_k, M^k) \right\} p^*(x_{K-1} | M^{K-1}) p^*(M^{K-1}) \quad (22)$$

The cardinality of a sequence M^k is $|\mathcal{M}|^k$, grows exponentially with k . Hence, each conditional in the product above is a table of many continuous densities.

Eliminating the last state x_{K-1} yields a new factor $\tau(M^{K-1})$ on the entire mode sequence:

$$\tau(M^{K-1}) = C_m \int_{x_{K-1}} q^*(x_{K-1}) \quad (23)$$

where $q^*(x_{K-1})$ is the unnormalized posterior density on x_{K-1} , and C_m is a mode-dependent constant that derives from the motion model and measurement factors in (4).

B. The Multi-hypothesis Smoother

The Bayes net chain (22) can be arranged in a data structure that has the same structure as the hypothesis tree from the MHT [24]. As discussed above, Equation 22 hides $|\mathcal{M}|^{K-1}$ different chains, one for each mode sequence. A

disadvantage of working with that representation is that the arity of each conditional increases over time, and the multi-hypothesis nature of the smoothing problem is hidden from view. However, because each conditional density on x_{k-1} only depends on the subset of modes $M^k \doteq \{m_i\}_0^{k-1}$, we can arrange the conditionals in a tree. As an example, the tree corresponding to Figure 4a is shown in Figure 4b.

Formally, the tree distributes every conditional density $p^*(x_{k-1} | x_k, M^k)$ in the switching Bayes net (22) over sets of $|\mathcal{M}|^{k-1}$ *single-mode* switching conditional densities, indexed by their mode history prefix M^{k-1} :

$$p^*(x_{k-1} | x_k, M^k) \doteq \{p_{M^{k-1}}^*(x_{k-1} | x_k, m_{k-1})\}_{M^{k-1}} \quad (24)$$

E.g., the first three conditionals correspond to these sets,

$$\begin{aligned} p^*(x_0 | x_1, m_0) &\doteq \{p_{M^0}^*(x_0 | x_1, m_0)\}_{M^0=\emptyset} \\ p^*(x_1 | x_2, m_0, m_1) &\doteq \{p_{M^1}^*(x_1 | x_2, m_1)\}_{M^1=0,1} \\ p^*(x_2 | x_3, m_0, m_1, m_2) &\doteq \{p_{M^2}^*(x_2 | x_3, m_2)\}_{M^2=00,01,10,11} \end{aligned}$$

which correspond exactly to the inner nodes shown in Figure 4b. The final layer in the tree is the set of densities on the final state x_{K-1} conditioned on the entire mode sequence M^{K-1} :

$$p^*(x_{K-1} | M^{K-1}) \doteq \{p_{M^{K-1}}^*(x_{K-1})\}_{M^{K-1}=\dots} \quad (25)$$

Recovering the optimized state sequence X^{K*} for any leaf node $p_{M^{K-1}}^*(x_{K-1})$ can be done simply by back-substitution in reverse time order, following the directed edges in the tree until the root. In particular, the estimate corresponding to the highest value of $\tau(M^{K-1})$ (Eqn. 23) corresponds to the MAP estimate. The corresponding optimal mode sequence M^{K-1*} can be recovered in a similar fashion, if one takes care to annotate the chosen mode on the edges in the tree.

C. Incremental Inference

In an incremental scheme this tree grows over time, as illustrated in Figures 5-7. At each incremental smoothing iteration, all of the leaves of the tree are replicated $|\mathcal{M}|$ times. Hence, we have to consider an exponentially growing number of hypotheses at each step.

However, extending each leaf node towards the future is simple and fast, and we can incrementally keep track of the probability of each mode sequence. In particular, after K steps, when estimating the next state x_K , assembly and elimination of the factor graph fragment proceeds as in Section II-D. We then use (23) to calculate $\tau(M^K)$ and *add* it to the previous value τM^{K-1} to get an updated τ value. Book-keeping is simple as each leaf only has to store one τ value: the number of leaves is exactly $|\mathcal{M}|^K$ after extending, which is the size of the new $\tau(M^K)$ table.

The integral (23) depends on the problem, but can be done in closed form in the linear-Gaussian case. In particular, the QR factorization (19) yields

$$q^*(x_K) = \exp \left\{ -\frac{1}{2} \|T_m x_K - v_m\|^2 - \frac{1}{2} e_m^T e_m \right\} \quad (26)$$

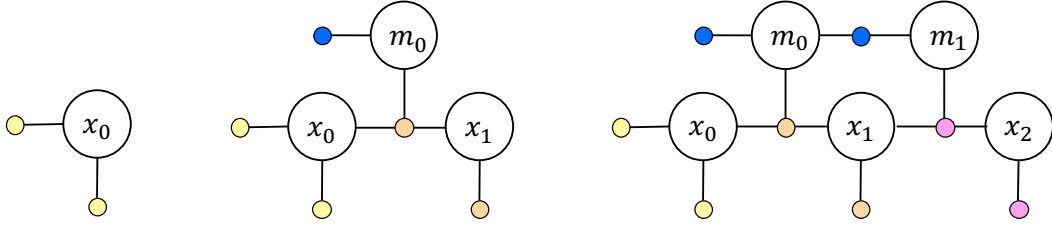


Fig. 5: Evolving factor graph during incremental inference.

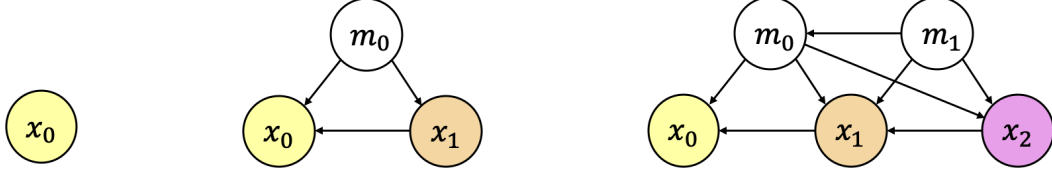


Fig. 6: Corresponding Bayes net resulting from eliminating (a).

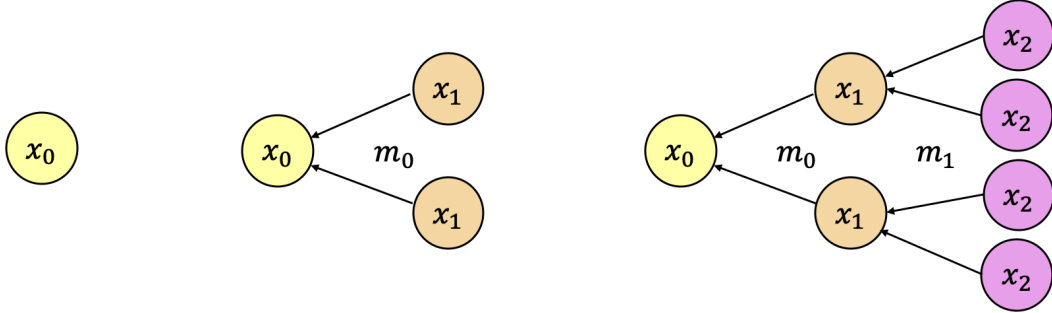


Fig. 7: Incremental Multi-hypothesis Smoother over time.

where the constant C_m derives from (12) and (13):

$$C_m = \sqrt{|\mathcal{I}_m \mathcal{I}_z|} \text{ where } \mathcal{I}_m = Q_m^{-1} \text{ and } \mathcal{I}_z = R_m^{-1} \quad (27)$$

Note that C_m can be omitted if the measurements and process covariances are not dependent on the mode m . With this, integration of (23) for the factor on the *extended* sequence M^K is given by

$$\tau(M^K) = \exp \left\{ -\frac{1}{2} e_m^T e_m \right\} \sqrt{\frac{|\mathcal{I}_m \mathcal{I}_z|}{|T_m^T T_m|}} \quad (28)$$

The first factor above penalizes error, and the latter is the ratio between the mode-dependent information in the factors (numerator) and the information in the posterior (denominator). The discrete factor $\tau(M^K)$, of size $|\mathcal{M}|^K$, can then be multiplied with $p(m_{K-1}|m_{K-2})$ into $p^*(M^{K-1})$ to yield the posterior $p^*(M^K)$ on the new mode sequence M^K .

Working in log-space avoids numerically unstable multiplication of many small numbers. Taking the negative log of (28) yields

$$\frac{1}{2} e_m^T e_m + \log |T_m| - \frac{1}{2} \log |\mathcal{I}_m \mathcal{I}_z| \quad (29)$$

where we made use of the fact that T_m is square.

D. Pruning and Marginalization

Unbounded computational cost can be avoided by setting a pruning threshold θ , and marginalizing out older states.

We chose a pruning scheme that evaluates the posterior on the mode sequence M^{K-1} *before* extending the leaves. Any leaf with an associated probability less than θ will not be extended. In practice we choose $\theta = 1\%$ or $\theta = 0.1\%$, which provides a good compromise between accuracy and computation in the examples we tried.

Marginalizing out older states, e.g., after a fixed lag N , is straightforward: we simply discard parts of the tree further than N levels from the current time step. Note that this can lead to the tree becoming a forest, but this is not an issue as leaves can continue to be expanded. Another scheme is to simply drop the nodes before the last fork. With aggressive pruning this can occur at a quite shallow depth.

Choosing a high value for N does not incur a high cost. The computational cost of keeping a linear chain before the last fork is zero, and memory load is linear in time. Note however that recovering optimal state sequences at each time does require computation. If this is needed, a wildfire threshold as in iSAM2 [13] can be adopted here as well.

E. Metrics

Finally, evaluating estimated mode sequences needs some care. Each leaf in the tree with parameters Θ corresponds to a hypothesis for the corresponding mode history. When given a ground truth mode sequence Y^{K-1} , we are faced with evaluating how good our estimate is with respect to

it. One metric is to evaluate the likelihood of our model Θ , which is proportional to the probability of producing the ground truth,

$$L(\Theta; Y^{K-1}) \propto P(Y^{K-1}|\Theta) = \int_{X^K} p(X^K, Y^{K-1}|Z^K) = p^*(Y^{K-1}) \quad (30)$$

which is exactly the leaf probability evaluated for Y^{K-1} . Typically an error is defined as the negative log of this, i.e.,

$$NLL_1(\Theta; Y^{K-1}) = -\log p^*(Y^{K-1}). \quad (31)$$

A more practical metric is to use the mode marginals. Since we prune hypotheses, and it is likely that the ground truth sequence is not among the unpruned branches, the error (31) is almost always infinite. A more practical error can be obtained by defining the mode marginals

$$p^*(M_k = m) = \sum_{M_{k,m}^{K-1}} p^*(M^{K-1}) \quad (32)$$

where $M_{k,m}^{K-1}$ is defined to be the set of all mode sequences having $m_k = m$. The negative log-likelihood of these marginals as a prediction on the ground truth yields the familiar categorical cross entropy loss:

$$NLL_2(\Theta; Y^{K-1}) = -\sum_k \log p^*(M_k = y_k). \quad (33)$$

IV. EXPERIMENTS

Below we demonstrate the generality of the incremental Multi-Hypothesis Smoother with examples in three problem domains: lane change detection (1D), aircraft maneuver detection (2D), and contact detection in legged robots (3D).

A. Lane Change Detection

The first example concerns lane change detection in a highway scenario. The trajectories were obtained from the NGSIM Interstate I-80 dataset, which consists of locations of vehicles travelling in a 503m test area on the I-80 highway recorded at 10 Hz. We modeled the lateral dynamics of a car using 2 distinct modes: Constant (CT) and Constant Velocity (CV). In both cases we use a linear model

$$p(x_k|x_{k-1}, m) = \mathcal{N}(x_k; F_m x_{k-1}, Q_m) \quad (34)$$

where the system matrices F_m we use are given by

$$F_{CT} = \begin{bmatrix} 1 & 0 \\ 0 & 0 \end{bmatrix}, F_{CV} = \begin{bmatrix} 1 & T \\ 0 & 1 \end{bmatrix} \quad (35)$$

with corresponding noise covariance matrices Q_m

$$Q_{CT} = \text{diag}(\sigma_{CT}^2, 0) \quad (36)$$

$$Q_{CV} = \text{diag}(0, \sigma_{CV}^2). \quad (37)$$

Fig. 8 shows the detected lane change events for a car driving changing lanes for 4 times in a 500m path.

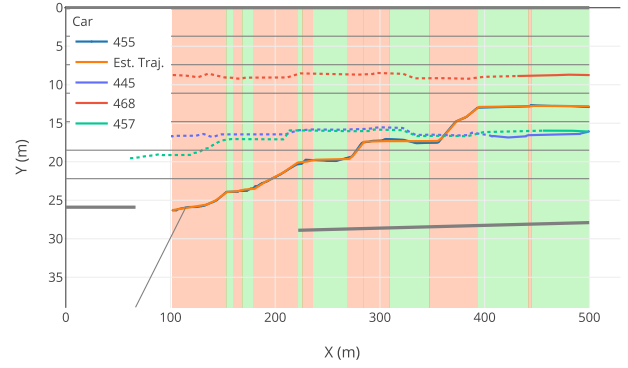


Fig. 8: Car trajectory with overlaid mode annotations. Green: CT, Red: CV.

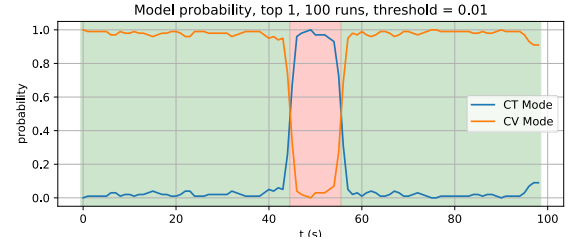


Fig. 9: Mode probability of 100 *Monte Carlo* runs of the iMHS algorithm on aircraft example.

B. Aircraft Maneuver Detection

To quantitatively evaluate the iMHS algorithm, we run the algorithm on the 2-mode switching aircraft tracking task from [11]. The aircraft model has 2 discrete modes, constant velocity (CV) and coordinated turn (CT). The dynamics of this model is given by the following set of discrete-time system equations:

$$x(k+1) = \begin{bmatrix} 1 & T & 0 & 0 \\ 0 & 1 & 0 & 0 \\ 0 & 0 & 1 & T \\ 0 & 0 & 0 & 1 \end{bmatrix} x(k) + \begin{bmatrix} \frac{T^2}{2} & 0 \\ T & 0 \\ 0 & \frac{T^2}{2} \\ 0 & T \end{bmatrix} u_i(k) + w_i(k) \quad (38)$$

$$y(k) = \begin{bmatrix} 1 & 0 & 0 & 0 \\ 0 & 0 & 1 & 0 \end{bmatrix} x(k) + v_i(k) \quad (39)$$

In our simulation, $w_i(k)$ and $v_i(k)$ are both zero-mean Gaussian process noise with a standard deviation of $[1, 1, 1, 1]^T$. For each mode, the two constant control inputs were assigned to be $u_{CV} = [0, 0]^T$ and $u_{CT} = [1.5, 1.5]^T$.

The results (Fig. 9) shows that the iMHS algorithm is able to accurately identify the two modes of flight. In the figure, the green and pink background colors indicate the ground truth mode. Note that the change of mode is identified without any delay, whereas filtering algorithms like RMIMM always have a delay ≥ 1 time step at state transitions [11].

To verify the performance of our system we can also run it as a filter. In this mode the algorithm runs online and outputs the current mode estimate as soon as a measurement is taken. We ran this configuration with the more complex trajectory

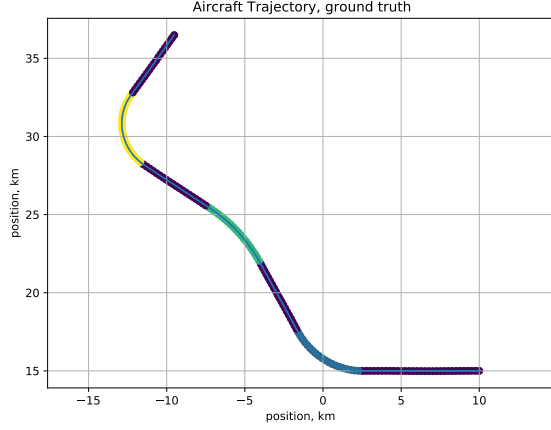


Fig. 10: A complex aircraft trajectory with 1 CV mode (blue segments) and 3 CT modes (colored).

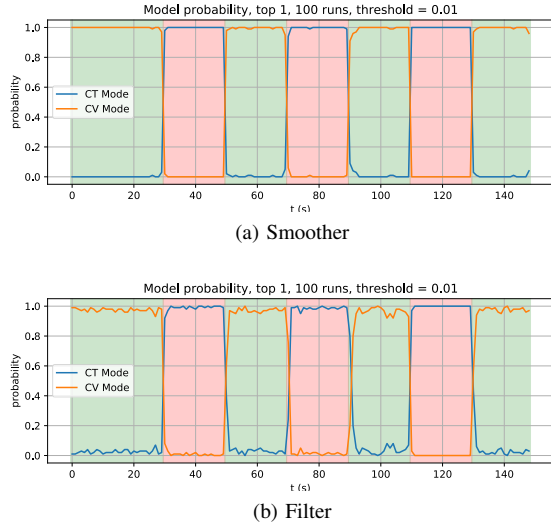


Fig. 11: Mode probability of 100 *Monte Carlo* runs of the iMHS algorithm in smoother mode v.s. filter mode (real-time) on a complex trajectory for the flight experiment.

from [11] shown in Fig. 10 which has 7 flight phases: 3 distinct CT modes each with a turn speed of $\omega = -3m/s$, $\omega = 1.5m/s$ and $\omega = -4.5m/s$. The plane starts from $(x = 10 \text{ km}, y = 15 \text{ km})$ with an initial speed of 246.93 m/s .

Comparison of Fig. 11a and Fig. 11b, show that the iMHS can robustly identify the modes even in the presence of a stochastic process and measurement noise. As expected, in the filter mode the current mode estimate is less accurate than the smoothing mode, due to the high level of noise present in the lateral channel. However, even in filter mode the iMHS algorithm still maintains $> 90\%$ accuracy throughout the trajectory even in filter mode.

C. Contact Estimation in Legged Robots

The final application we investigated is inferring the contact state of a quadrupedal robot. We used both simulated



Fig. 12: The ANYbotics ANYmal B quadrupedal robot at Keble College, Oxford, United Kingdom.

Platform	LH	LF	RF	RH
A1 Simulation	1.013	1.089	0.377	1.242
ANYmal Data	0.819	0.639	1.362	1.284

TABLE I: Cross-entropy error. This measures the difference between our estimated contact states and the pseudo-ground-truth states. Lower values indicate better performance.

data from an A1 and actual log data from an ANYbotics ANYmal quadruped (Fig. 12) walking in Keble College, Oxford. The latter robot and its sensors are described in [27], and the dataset we used comprises of several trotting sequences around a courtyard. The robot's state estimator [3] gives us the position of the base link T_B^O and the feet p_i^O in an odometry frame O that is initialized at the start of a run and updated using an internal state estimator.

We frame the problem as estimating the foot trajectory jointly with the contact sequence M^{K-1} where the mode at time t_k is binary, indicating contact with the ground. We model the motion of a foot during contact as a 3-dimensional Gaussian density, whose parameters μ_C^O and Σ_C are estimated from training runs. This leads to a quadratic factor between successive foot positions p_{k-1}^O and p_k^O

$$f_k^C(p_{k-1}^O, p_k^O) = \|p_k^O - p_{k-1}^O - \mu_C^O\|_{\Sigma_C}^2, \quad (40)$$

which is expected to have zero mean with a tight covariance. During swing, however, we model a constraint on the foot positions p_k^B in the *base* frame, reflecting our knowledge that the feet move rigidly with respect to the body during swing. We obtain:

$$f_k^S(p_{k-1}^O, p_k^O) = \|T_{O,k}^B p_k^O - T_{O,k-1}^B p_{k-1}^O - \mu_S^B\|_{\Sigma_S}^2$$

where we made use of $p_k^B = T_{O,k}^B p_k^O$, with $T_O^B = (T_B^O)^{-1}$. We have $T_O^B p^O = T_O^R p^O + t_B^O$ and we assume $R_{O,k}^B \approx R_{O,k-1}^B$, which allows us to simplify this into another quadratic factor,

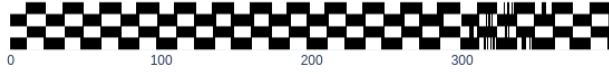
$$f_k^S(p_{k-1}^O, p_k^O) = \|p_k^O - p_{k-1}^O - (\Delta t_{B,k-1,k}^O + R_{B,k}^O \mu_S^B)\|_{\Sigma_S}^2.$$

where $\Delta t_{B,k-1,k}^O = t_{B,k}^O - t_{B,k-1}^O$.

Qualitative results for the A1 simulation and the Keble dataset are shown in Figures 13 and 14, respectively. For



(a) Gait Marginal Probabilities



(b) Gait MAP Estimate



(c) Gait Error

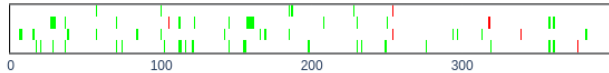
Fig. 13: A1 simulation results. Panel (a) and (b) represents the marginal probabilities (32) and the MAP estimate for the contact sequence of all feet, with black signifying contact. Panel (c) is the error for the MAP estimate, color-coded with red for incorrectly predicted contact, green for incorrectly predicted flight, and white for no error.



(a) Gait Marginal Probabilities



(b) Gait MAP Estimate



(c) Gait Error

Fig. 14: ANYmal B. See caption of Figure 14

quantitative evaluation we use the contact states provided by the probabilistic contact detector from [12] as pseudo-ground-truth. As described in Section III-E we report on the categorical cross-entropy error between the contact state marginals estimated by the iMHS and the ground truth contact states in Table I.

V. CONCLUSIONS

The incremental Multi-Hypothesis Smoother proposed in this paper provides a solid foundation for inference over time in hybrid dynamical systems. Our results above demonstrate the applicability in various domains, but we are most excited about the possibility of integrating this with a state of the art inertial state estimation pipeline. This would enable state estimation in a variety of legged robots without the need for

contact sensors or dedicated force sensors. Smoothing rather than filtering will enable state estimators to more accurately update continuous states that depend on hybrid states.

REFERENCES

- [1] Y. Bar-Shalom, X.-R. Li, and T. Kirubarajan. *Estimation with Applications to Tracking and Navigation*. John Wiley & Sons, Inc., New York, USA, 2001.
- [2] G. J. Bierman. Sequential square root filtering and smoothing of discrete linear systems. *Automatica*, 10(2):147–158, Mar. 1974.
- [3] M. Blösch, M. Hutter, M. A. Höpflinger, S. Leutenegger, C. Gehring, C. D. Remy, and R. Siegwart. State estimation for legged robots - consistent fusion of leg kinematics and imu. *RSS*, 2012.
- [4] I. J. Cox and S. L. Hingorani. An efficient implementation of Reid's multiple hypothesis tracking algorithm and its evaluation for the purpose of visual tracking. *IEEE Transactions on Pattern Analysis and Machine Intelligence*, 18(2):138–150, Feb. 1996.
- [5] F. Dellaert and M. Kaess. Factor Graphs for Robot Perception. *Foundations and Trends in Robotics*, 6(1-2):1–139, 2017.
- [6] Z. Dong, B. A. Seybold, K. P. Murphy, and H. H. Bui. Collapsed amortized variational inference for switching nonlinear dynamical systems. In *ICML*, page 10, 2020.
- [7] P. Eide and P. Maybeck. An MMAE failure detection system for the F-16. *IEEE Transactions on Aerospace and Electronic Systems*, 32(3):1125–1136, July 1996.
- [8] J. W. Grizzle, C. Chevallereau, R. W. Sinnet, and A. D. Ames. Models, feedback control, and open problems of 3D bipedal robotic walking. *Automatica*, 50(8):1955–1988, Aug. 2014.
- [9] P. Hanlon and P. Maybeck. Multiple-model adaptive estimation using a residual correlation Kalman filter bank. *IEEE Transactions on Aerospace and Electronic Systems*, 36(2):393–406, Apr. 2000.
- [10] M. Hsiao and M. Kaess. MH-iSAM2: Multi-hypothesis iSAM using Bayes Tree and Hypo-tree. In *2019 International Conference on Robotics and Automation (ICRA)*, pages 1274–1280, Montreal, QC, Canada, May 2019. IEEE.
- [11] I. Hwang, H. Balakrishnan, and C. Tomlin. State estimation for hybrid systems: Applications to aircraft tracking. *IEEE Proceedings - Control Theory and Applications*, 153(5):556–566, Sept. 2006.
- [12] F. Jenelten, J. Hwangbo, F. Tresoldi, C. D. Bellicoso, and M. Hutter. Dynamic locomotion on slippery ground. *IEEE Robotics and Automation Letters*, 4(4):4170–4176, 2019.
- [13] M. Kaess, H. Johannsson, R. Roberts, V. Ila, J. J. Leonard, and F. Dellaert. iSAM2: Incremental smoothing and mapping using the Bayes tree. *The International Journal of Robotics Research*, 31(2):216–235, Feb. 2012.
- [14] M. Kaess, A. Ranganathan, and F. Dellaert. iSAM: Fast Incremental Smoothing and Mapping with Efficient Data Association. In *Proceedings 2007 IEEE International Conference on Robotics and Automation*, pages 1670–1677, Rome, Italy, Apr. 2007. IEEE.
- [15] M. Kaess, A. Ranganathan, and F. Dellaert. iSAM: Incremental Smoothing and Mapping. *IEEE Transactions on Robotics*, 24(6):1365–1378, Dec. 2008.
- [16] Z. Khan, T. Balch, and F. Dellaert. MCMC-Based Particle Filtering for Tracking a Variable Number of Interacting Targets. *IEEE Transactions on Pattern Analysis and Machine Intelligence*, page 34, 2005.
- [17] Z. Khan, T. Balch, and F. Dellaert. MCMC Data Association and Sparse Factorization Updating for Real Time Multitarget Tracking with Merged and Multiple Measurements. *IEEE Transactions on Pattern Analysis and Machine Intelligence*, 28(12):13, 2006.
- [18] P. S. Maybeck. *Stochastic Models, Estimation and Control*. Academic Press, 1979.
- [19] K. P. Murphy. Switching Kalman Filters. Technical report, U.C. Berkeley, 1998.
- [20] K. P. Murphy. *Dynamic Bayesian Networks: Representation, Inference and Learning*. PhD thesis, U.C. Berkeley, 2002.
- [21] S. Oh, S. Russell, and S. Sastry. Markov Chain Monte Carlo Data Association for Multi-Target Tracking. *IEEE Transactions on Automatic Control*, 54(3):481–497, Mar. 2009.
- [22] S. M. Oh, J. Rehg, T. Balch, and F. Dellaert. Learning and inference in parametric switching linear dynamic systems. In *Tenth IEEE International Conference on Computer Vision (ICCV'05) Volume 1*, pages 1161–1168 Vol. 2, Beijing, China, 2005. IEEE.

- [23] S. M. Oh, J. M. Rehg, T. Balch, and F. Dellaert. Data-Driven MCMC for Learning and Inference in Switching Linear Dynamic Systems. In *AAAI*, page 6, 2005.
- [24] D. Reid. An algorithm for tracking multiple targets. *IEEE Transactions on Automatic Control*, 24(6):843–854, Dec. 1979.
- [25] R. L. Streit and T. E. Luginbuhl. Probabilistic multi-hypothesis tracking. Technical report, Naval Undersea Warfare Center Division, Feb. 1995.
- [26] J. Vermaak, S. Godsill, and P. Perez. Monte Carlo filtering for multi target tracking and data association. *IEEE Transactions on Aerospace and Electronic Systems*, 41, Jan. 2005.
- [27] D. Wisth, M. Camurri, and M. Fallon. Robust legged robot state estimation using factor graph optimization. *IEEE Robotics and Automation Letters*, 4(4):4507–4514, 2019.
- [28] W. Wu, M. Black, D. Mumford, Y. Gao, E. Bienenstock, and J. Donoghue. Modeling and Decoding Motor Cortical Activity Using a Switching Kalman Filter. *IEEE Transactions on Biomedical Engineering*, 51(6):933–942, June 2004.
- [29] J. L. Yepes, I. Hwang, and M. Rotea. New Algorithms for Aircraft Intent Inference and Trajectory Prediction. *Journal of Guidance, Control, and Dynamics*, 30(2):370–382, Mar. 2007.